# A NON-LINEAR, TWO-STEP ESTIMATION ALGORITHM FOR CALIBRATING SOLID-STATE STRAPDOWN MAGNETOMETERS

D. Gebre-Egziabher*, G. H. Elkaim†, J. D. Powell‡ and B. W. Parkinson§
Department of Aeronautics and Astronautics, Stanford University

**Key Words**: Magnetometer, Heading, Non-Linear Estimation

## Abstract

This paper presents a new algorithm for calibrating modern, solid-state strapdown magnetometers. The traditional method for calibrating these sensors is a cumbersome procedure called "swinging" which involves leveling and rotating the vehicle containing the magnetometer through a series of known headings. The calibration procedure presented in this paper does not require any external reference. Furthermore, unlike the method of "swinging", this calibration method performs the calibration in the magnetic field domain and not the heading domain. This makes the algorithm applicable for cases where the magnetometer is used in applications other than heading determination.

The calibration algorithm uses an estimator where the states are the various sensor errors. These states in the estimator are hard iron biases, soft iron biases, and scale factor errors. This calibration procedure is implemented using a non-linear two step estimator where the first step problem is solved by using standard batch least squares linear estimation techniques and the second step is solved algebraically. This two step estimator outperforms an Extended Kalman Filter (EKF) formulation.

A low-cost magnetometer triad was used to collect data and experimentally validate the calibration algorithm. The non-linear two step estimator results in magnetometer calibration residual less than 0.005 Gauss which translates to heading errors on the order of 1 degree.

## Introduction

Magnetometers are instruments used for measuring the strength and direction of magnetic fields. They are used extensively in airplane navigation applications for determination of vehicle heading where heading is defined to be the angle formed between the longitudinal axis of an airplane and magnetic north. In aviation applications, what is normally used is a pair of magnetometers mounted perpendicular to each other or a triad of magnetometers mounted orthogonally. In this configuration, the magnetometers are used to measure the strength of the earth's magnetic field vector in body coordinates from which heading is computed. When the vehicle is straight and level (pitch and roll angles equal zero), heading is determined using:

$$\psi = -\arctan\left(\frac{B_y^b}{B_x^b}\right) \tag{1}$$

where $B_x^b$ and $B_y^b$ represent measurements of the earth's magnetic field vector resolved in a coordinate system attached to the aircraft's body. The superscript "b" denotes a vector measurement made in the body coordinate frame. Errors in making the measurements $B_x^b$ and $B_y^b$ directly corrupt the accuracy of the heading obtained from Equation 1. The process of calibrating magnetometers involves identifying and removing the errors in these measurements. This paper introduces a new algorithm for performing magnetometer calibration. In Section 1, a detailed description of the errors that affect magnetometer readings will be discussed. In Section 2, prior art in the calibration of magnetometers will be presented. This discussion will include

*Research Assistant, gebre@stanford.edu
†Research Assistant, elkaim@stanford.edu
‡Ph.D., Professor, jdpowell@stanford.edu
§Ph.D., Professor, brad@relgyro.stanford.edu

a previous method for calibrating magnetometers. This older method of calibrating magnetometers has difficulties that are resolved using the new algorithm. In Section 3, the new two-step estimation technique for calibrating magnetometers will be presented. In Section 4, we present simulation studies that document the performance of the new algorithm. In Section 5, experimental results will be presented. We conclude the paper in Section 6 by presenting a summary.

# 1 Magnetometer Measurement Error Models

Magnetometers come in many different forms and operate on different principles. A new generation of low-cost magnetometers used in this research are Anisotropic Magnetoresistive (AMR) sensors. These sensors have a sensing element that is made form a nickel-iron alloy (or Permalloy) whose electrical resistance changes in the presence of magnetic fields. The Permalloy material is normally deposited on thin silicon wafers which can be bulk manufactured and in a form factor suitable for commercial integrated circuit packages. The sensing element of the magnetometer used in this research has dimensions on the order of 10 mm on a side [1]. The output of these devices is an analog voltage proportional to the strength of the magnetic field.

The mathematical model for the output error of such strapdown magnetometer triads is:

$$\hat{\vec{B}}^b = C_m \, C_{sf} \, C_{si} \, \left( \vec{B}^b + \delta \vec{B}^b \right). \tag{2}$$

In Equation 2, $\vec{B}^b$ represents the *actual* or true magnetic field vector while $\hat{\vec{B}}^b$ represents the *measured* magnetic field vector. $\delta \vec{B}^b$ in Equation 2 represents the hard iron biases. The matrix $C_{si}$ accounts for the soft iron errors and $C_{sf}$ is a matrix to account for scale factor errors. Finally, the matrix $C_m$ represents misalignment errors. Each one of these error terms is discussed in detail below.

## 1.1 Hard Iron Errors: $\delta \vec{B}^b$

The magnetic field that is used in heading determination is the earth's magnetic field. In most practical applications there will be other unwanted magnetic fields corrupting the measurements of the magnetometer triad. These unwanted fields are normally generated by ferromagnetic materials with permanent magnetic fields (or "hard irons") that are part of the aircraft structure or equipment installed near the magnetometer. These unwanted magnetic fields are superimposed on the output of the magnetometers' measurement of the earth's magnetic field. The effect of this superposition is to bias the magnetometer output.

If the unwanted magnetic fields are time invariant, then they are called "hard iron" errors and can be represented by a vector quantity $\delta \vec{B}^b$. If the strength and direction of these unwanted magnetic fields is known, then their effect can be removed to unbias the magnetometer readings. It should be noted that the unwanted magnetic fields can also be caused by items external to the aircraft, but usually the aircraft is moving and the effect of such fields will be temporary. Furthermore, fields due to sources external to the aircraft will be present only is when the aircraft is on the ground. Thus, errors due to external fields can be safely neglected. Items inside can generate unwanted magnetic fields that are time varying. For example, such an item would be a current carrying wire. If the current through the wire is time varying, the resulting magnetometer bias will also be time varying and difficult to calibrate. Fortunately, such errors can be eliminated by taking care during installation of the magnetometers.

## 1.2 Soft Iron Errors: $C_{si}$

There are materials that generate magnetic fields in response an externally applied fields. The field generated by these materials, called "soft irons", can vary over a wide range depending on both the magnitude and direction of the applied external magnetic field. If such materials are present, they will generate a magnetic field that will be superimposed on the magnetometer output as they generate their own magnetic field in response to the earth's magnetic field. Since the orientation of the earth's magnetic field vector relative to the soft iron materials fixed inside the aircraft changes with aircraft attitude, this gives rise to a varying bias on the magnetometer output.

In a simple one-dimensional case the magnitude of the soft iron response is proportional to the external magnetic field. The constant of proportionality is a property of the soft iron material and it is referred to as the material's magnetic susceptibility. In this work it will be assumed that this simple linear relationship is sufficient. However, in some cases there can be appreciable hysteresis. In most soft iron materials the hysteresis is small enough that the linear model is sufficient. In a

hysteresis-free, three-dimensional case, a $3 \times 3$ matrix is required as opposed to a constant of proportionality . This is the $C_{si}$ matrix in Equation 2. In most aircraft installations, magnetometers are installed in parts of aircraft where errors due to soft iron will be small, and thus, for the work in this paper, we assume that $C_{si}$ is an identity matrix.

### 1.3 Scale Factor Errors: $C_{sf}$

Ideally, the three magnetometers that make up the triad are identical. In reality, however, this may not be the case; each magnetometer will have different sensitivities. That is, when all three magnetometers are subjected to an identical magnetic field, the observed output from each will not be the same due to scale factor errors. Calibrating the scale factor error involves determining the multiplicative factor that has to be applied to each magnetometer such that the outputs will be the same when subjected to identical magnetic fields. In the three-dimensional case, the multiplicative constant is the $3 \times 3$ matrix $C_{sf}$.

### 1.4 Misalignment Errors: $C_m$

In an ideal installation, the magnetometer triad will be mounted in perfect alignment with the body axis of the aircraft. If reasonable alignment is not achieved, however, errors in the magnetometers' output will be present due to cross coupling of the magnetic field axes. If care is taken during the installation process, the misalignment between the triad and the airplane body axes can be minimized. For the analysis that follows we assume that the magnetometer alignment is perfect and hence the term $C_m$ in Equation 2 is an identity matrix. Thus, in this work, and indeed in most aviation applications, the two error sources that magnetometer calibration algorithms have to deal with are hard iron biases and scale factor errors.

## 2 Prior Art–Calibration in the Heading Domain

Two-magnetometer heading determination systems have been used extensively in navigation applications. Traditionally the sensors used in these systems were flux-gate or flux-valve magnetometers. The method of calibration in the heading domain has been known for a long time [2] and has been used to calibrate modern solid-state magnetometers. This method of calibration is based on perturbation of the basic heading Equation 1 and a substitution of the error Equations 2. This results in the following heading error equation:

$$\delta\psi = A + B\sin(\psi) + C\cos(\psi) + D\sin(2\psi) + E\cos(2\psi). \tag{3}$$

Equation 3 is effectively a truncated Fourier series where the Fourier coefficients are functions of the hard and soft iron errors. Estimation of the Fourier coefficients is accomplished by a procedure called "swinging". The procedure involves leveling and rotating the vehicle containing the magnetometer through a series of $N$ *known* headings as shown schematically in Figure 1. At each known $k^{th}$ heading, the heading error $\delta\psi_k$ is computed which will be used to form the system of Equations 4. A batch least squares solution of Equation 4 yield estimates for the coefficients A through E.

$$\begin{bmatrix} \delta\psi_1 \\ \delta\psi_2 \\ \vdots \\ \delta\psi_N \end{bmatrix} = \begin{bmatrix} 1 & \sin(\psi_1) & \cos(\psi_1) & \sin(2\psi_1) & \cos(2\psi_1) \\ 1 & \sin(\psi_2) & \cos(\psi_2) & \sin(2\psi_2) & \cos(2\psi_2) \\ \vdots & & \ddots & & \vdots \\ 1 & \sin(\psi_N) & \cos(\psi_N) & \sin(2\psi_N) & \cos(2\psi_N) \end{bmatrix} \begin{bmatrix} A \\ B \\ C \\ D \\ E \end{bmatrix} \tag{4}$$

There are three major drawbacks with this calibration method which necessitated the development of the new calibration algorithm discussed in this paper. A shortcoming of the method which becomes apparent when examining Equations 3 is that heading is a required input. Since heading errors due to hard and soft iron errors are not constant but heading dependent, the heading input into the algorithm will be corrupted by a non-constant bias. Thus, another independent measurement of heading is required when calibrating magnetometers by this method. When performing this calibration for a magnetometer triad installed in an aircraft, the standard practice is to use a compass rose painted on the tarmac as shown in Figure 1 as the secondary independent heading measurement. The second drawback is that some of the coefficients A through E are functions of the local earth magnetic field strength. That is, if the vehicle with the magnetometers is expected to travel over a large geographic area, there will be large variations in the the local earth magnetic field vector and multiple calibrations must be performed. Each calibration will yield a location dependent coefficient set A through E that can be schedule as needed. Lastly, if the magnetometers are not going to be used in a heading determination system or if the system consists of three orthogonal magnetometers, then this calibration algorithm is not applicable.

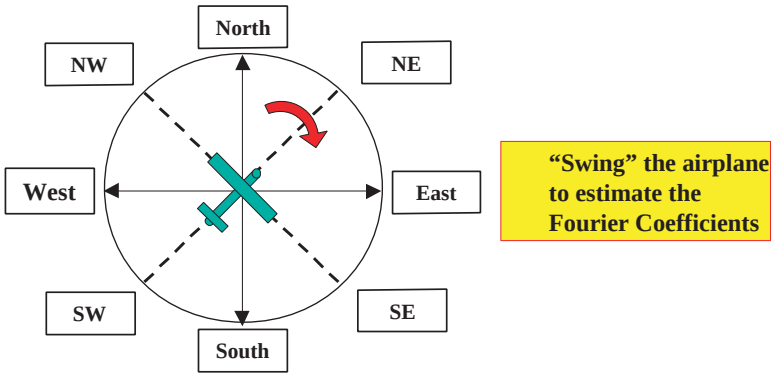


Figure 1: Graphical Description of Swinging.

# 3 Algorithm Development

This section presents the non-linear estimation technique which is the subject of this paper. Unlike the calibration algorithm presented before, this algorithm is not location dependent nor does it require an external heading reference. This calibration method is based on the fact that the locus of error-free measurements from two perpendicularly mounted magnetometers is a circle. It is easy to show this by examining the following equation:

$$B_x^{b\,2} + B_y^{b\,2} = B_H^2 \cos^2\psi + B_H^2 \sin^2\psi = B_H^2. \tag{5}$$

In the equation above, $B_H$ is the magnitude of the horizontal component of the earth's magnetic field vector. Equation 5 is the equation of a circle with its center at the origin. The radius of the circle is equal to the magnitude of the horizontal component of the local earth's magnetic field vector. The magnitude of the radius varies with latitude, longitude and altitude because the earth's magnetic field vector varies with geographic location. This variation of the earth's magnetic field vector is well known and well modeled. In this work a the magnitude of the local earth's magnetic field vector was determined using the 1999 International Geomagnetic Reference Field model [3].

The effect of the various magnetometer errors described in Equation 2 is to alter the shape of the circle described in Equation 5. Hard iron errors, for example, shift the origin of the circle. This can be shown mathematically if we consider the case where the x and y components of the earth's magnetic field vector are offset by hard iron biases $\delta B_{x_0}$ and $\delta B_{y_0}$ respectively. In this case, the measured field strengths $\hat{B}_x^b$ and $\hat{B}_y^b$ are given by:

$$\hat{B}_x^b = \delta B_x + B_x^b \tag{6}$$
$$\hat{B}_y^b = \delta B_y + B_y^b. \tag{7}$$

Thus, the equation for the locus of the magnetometer measurements becomes:

$$\left(\hat{B}_x^b - \delta B_{x_0}\right)^2 + \left(\hat{B}_y^b - \delta B_y\right)^2 = B_H^2. \tag{8}$$

This is still the equation of a circle but one having its center located at $(\delta B_{x_0}, \delta B_{y_0})$. Scale factor errors cause the body x- and y- magnetometer measurements to be different when both are subjected to a magnetic field of the same strength. This can be expressed mathematically as follows:

$$\hat{B}_x^b = (1 + sf_x)\, B_H \cos\psi \tag{9}$$
$$\hat{B}_y^b = -(1 + sf_y)\, B_H \sin\psi \tag{10}$$

which can be rearranged and written as:

$$\left(\frac{\hat{B}_x^b}{1 + sf_x}\right)^2 + \left(\frac{\hat{B}_y^b}{1 + sf_y}\right)^2 = B_H{}^2, \tag{11}$$

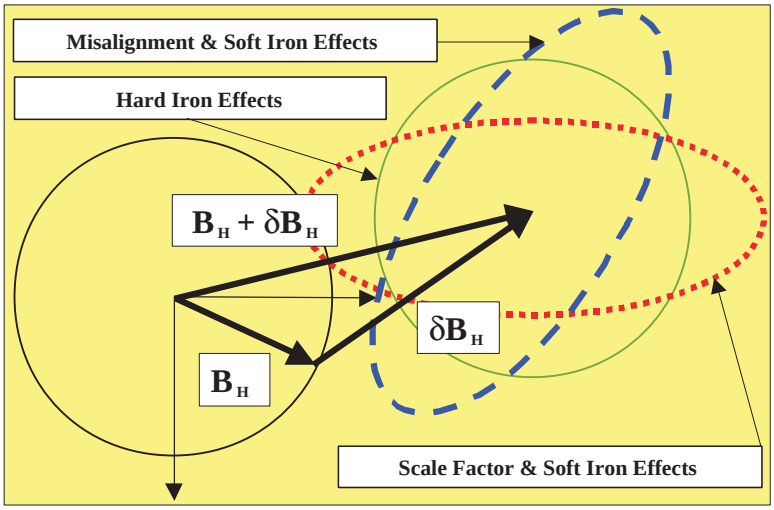


Figure 2: Effect of Errors on Magnetic Field Measurement Locus in 2-D.

which is the equation of an ellipse centered at the origin. The major and minor axes magnitudes are determined by the scale factor errors $sf_x$ and $sf_y$. When the magnetometer output is corrupted by scale factor errors as well as hard iron error biases $\delta B_{x_0}$ and $\delta B_{y_0}$, the resulting locus is an ellipse with its center at $\delta B_{x_0}$ and $\delta B_{y_0}$. Mathematically, this is given by:

$$\left(\frac{\hat{B}_x^b - \delta B_{x_0}}{1+sf_x}\right)^2 + \left(\frac{\hat{B}_y^b - \delta B_{y_0}}{1+sf_y}\right)^2 = {B_H}^2, . \tag{12}$$

Even though, as stated earlier, we will not be considering misalignment errors, we note that the effect of these errors on the locus of magnetometer measurements is to rotate the major and minor axes of the ellipse. Figure 2 is a graphical summary of the effect of the various errors on the locus of magnetometer measurements.

The calibration algorithm developed is a parameter estimation problem. When an aircraft with a pair of magnetometers is rotated through $360^\circ$ about its yaw axis, the locus of body fixed measurements will be an ellipse. The algorithm is an attempt to fit the best ellipse (in the least squares sense) to the measured data. If misalignment and soft iron errors are minimized during installation, then the parameter estimation unknowns are the hard iron errors and scale factor errors. In terms of the mathematics of the estimation process, the hard iron errors correspond to the center of the ellipse and the scale factor errors correspond to the size of the major and minor axes of the ellipse. Furthermore, extension of this algorithm to the case of three magnetometers is straight forward: instead of the parameters of an ellipse, the parameters of an ellipsoid are estimated.

There are two ways to carry out the parameter estimation. The first method is to use a classical approach to estimating parameters in a non-linear system of equations such as the Extended Kalman Filter (EKF) described in [4] and [5]. Specifically, this estimator is based on linearizing the locus described in Equation 12. The governing non-linear equations are linearized such that the perturbations of the parameter of interest are estimated. The estimated perturbations are added to non-perturbed variables and the estimation is repeated until convergence is achieved. It is an iterative procedure and requires a good initial guess of the scale factors and hard iron biases to start-off the algorithm. A series of simulation studies were performed and showed that this algorithm is primarily sensitive to three effects. Firstly, a reasonably close guess of the scale factors and hard iron biases is required. Initial guesses that are not close lead to divergence. Secondly, large amounts of sampling noise tended to cause the algorithm to diverge. The amount of noise that can be tolerated was a function of the third sensitivity factor: the portion of a complete ellipsoid available for estimation purposes. If a smaller portion of the ellipsoid is present in the data, very small amounts of noise are tolerated. If large amounts of the ellipsoid are present, then large amounts of noise can be handled.

The non-linear, two-step estimator, which solves the parameter identification problem by breaking the estimation process into two steps, is an adaptation of the estimator introduced in [6]. In the first step, a set of variable which are are called first step states are defined as a combination of the various parameters to be estimated. The estimation problem is linear in these first step state variables and, therefore, retains the desirable properties of linear systems. Following estimation of the first step

states, the second step states, which are the scale factors and hard iron biases, are extracted from the first state steps through algebraic manipulation.

Derivation of the equations for the non-linear, two-step estimator begin by expanding the locus equation. In this case we will deal with the three dimensional analog of Equation 12 which, when expanded, leads to the following:

$$\begin{aligned} R^2 &= \frac{(\hat{B}_x^b)^2 - 2(\hat{B}_x^b)(\delta B_{x0}) + (\delta B_{x0})^2}{(1+sf_x)^2} \\ &+ \frac{(\hat{B}_y^b)^2 - 2(\hat{B}_y^b)(\delta B_{y0}) + (\delta B_{y0})^2}{(1+sf_y)^2} \\ &+ \frac{(\hat{B}_z^b)^2 - 2(\hat{B}_z^b)(\delta B_{z0}) + (\delta B_{z0})^2}{(1+sf_z)^2} \end{aligned} \tag{13}$$

Equation 13 can be rearranged in put into matrix notation in the following manner:

$$-(\hat{B}_x^b)^2 = \begin{bmatrix} -2\hat{B}_x^b & (\hat{B}_y^b)^2 & -2\hat{B}_y^b & (\hat{B}_z^b)^2 & -2\hat{B}_z^b & 1 \end{bmatrix} \begin{bmatrix} \delta B_{x0} \\ k_2 \\ k_2(\delta B_{y0}) \\ k_3 \\ k_3(\delta B_{z0}) \\ k_4 \end{bmatrix} \tag{14}$$

Equation 14 represents one measurement point. If all the data collected from the magnetometer triad is assembled in the form shown in Equation 14, then we have a system of equations that can be solved for the unknown first step states which are the entries in the right-most hand vector in Equation 14. The auxiliary variables $k_1$ through $k_4$ are defined as follows:

$$k_1 = R^2(1+sf_x)^2 \tag{15}$$

$$k_2 = \frac{(1+sf_x)^2}{(1+sf_y)^2} \tag{16}$$

$$k_3 = \frac{(1+sf_x)^2}{(1+sf_z)^2} \tag{17}$$

$$k_4 = (\delta B_{x0})^2 + k_2(\delta B_{y0})^2 + k_3(\delta B_{z0})^2 - k_1 \tag{18}$$

Once the first step states are estimated, the scale factors and hard iron biases are extracted from the first step states algebraically by using the auxiliary variables.

# 4 Simulation Studies

The results of simulation studies to assess the performance of the two dimensional algorithm are pictured in Figure 3. The conclusions of these simulations can be extended to the three dimensional case. The simulation consisted of generating a circle of a specified radius. This circle corresponds to the trace of the locus of the earth's magnetic field vector in the horizontal plane. The circle was shifted from the origin by applying biases, deformed by applying non-uniform scale factors and finally corrupted by wide-band sensor noise. The circle and its altered counter parts are shown in Figure 3. The calibration algorithm is exercised on the sampled, corrupted points shown in grey in Figure 3. The calibration algorithm estimates the offset from the origin (hard iron biases) and the ellipticity (scale factors). The adjusted circle based on the estimation is shown in Figure 3. It should be noted that only a portion of the circle is adequate for estimation.

# 5 Results

In the previous section it was shown in simulation studies that the calibration algorithm works well. A final verification of this algorithm was carried out on experimental data. The data was collected from the experimental set up shown in Figure 4 where a triad of low-cost magnetometers were strapped on to a long wooden boom. This ensured that the magnetic fields generated by the data collection hardware did not introduce a time varying magnetic field that interfered with the experiments.

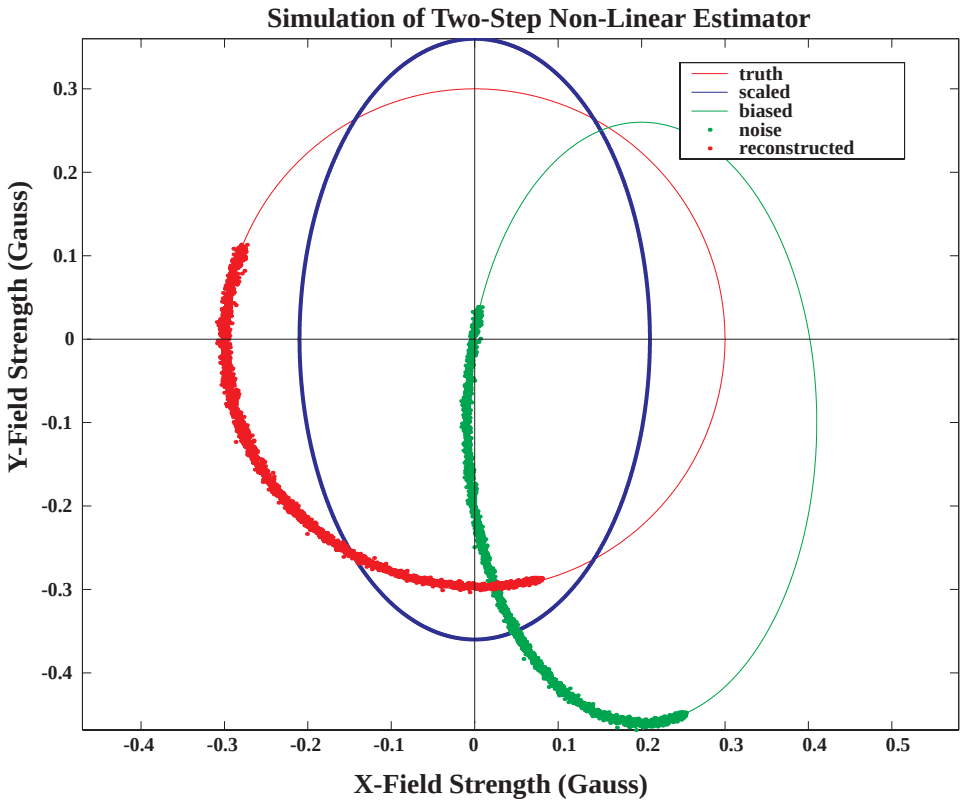


Figure 3: Performance of the Two-Step Estimator (Simulation).

One test was to compare the heading solution generated by the magnetometers with the heading solution from an expensive navigation grade Inertial Navigation System (INS). The INS is a Honeywell YG-1851 having rate gyros with rate drifts less than 0.01 deg/hr.

Figure 5 shows some of the data collected from this experiment. In the vicinity of San Francisco, CA, where this experiment was conducted, the earth's magnetic field vector has a magnitude of approximately 0.5 Gauss. Thus, for a perfectly calibrated magnetometer triad, all of the measurements should lie on a sphere with radius of 0.5 Gauss. This would be the larger or outer sphere shown in Figure 5. Due to hard iron and scale factor errors, the data lies near to a sphere with a smaller radius and offset from the origin. The calibration procedure generates the required parameters to place the data on a sphere of radius of 0.5 Gauss. The post calibration residuals are calculated to be on the order of 0.005 Gauss as shown on Figure 6. The residuals are slightly larger towards the right end of the plot. This is due to dynamics: at this point in the experiment the wooden boom carrying the magnetometers was being heavily loaded and likely flexed. Figure 7 shows the magnitude of the measured magnetic field vector before and after the calibration. The magnitude of the field vector before the calibration is seen to vary while the post calibration field magnitude is a constant 0.5 Gauss. The final comparison for calibration accuracy was performed in the heading domain. The heading error residual, which was computed by taking the difference between the heading solution generated by the calibrated magnetometer triad and the high quality INS, was found to have a standard deviation of approximately $3^\circ$. This residual error was in the form of wide-band noise which could be easily filtered by using a low-pass filter if this heading information was being used for vehicle guidance.

# 6 Conclusions

A non-linear two-step estimation algorithm for calibrating solid-state strapdown magnetometers was presented. This calibration algorithm allowed estimation of magnetometer errors. The estimated errors are subsequently used to calibrate the magnetometer. The procedure for estimating the magnetometer errors does not require any external heading reference. This

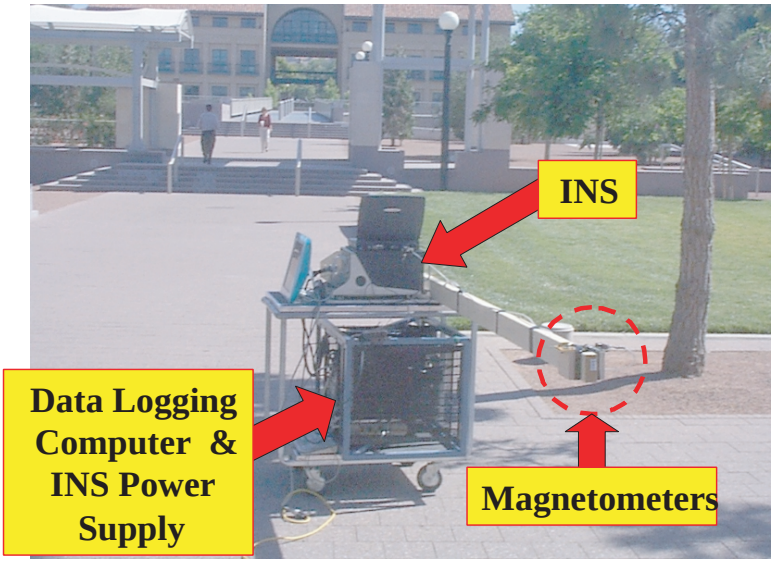


Figure 4: Experimental Setup for Ground Test.

calibration technique is both robust and accurate. The robustness was demonstrated experimentally by convergence even in the presence of considerable sensor noise. A further demonstration of the robustness of this algorithm is by the fact that only a small portion of the ellipsoid locus is required for the estimation process to work.

## 7 Acknowledgments

We wish to acknowledge the FAA Satellite Navigation Product Team and The Office of Technology and Licensing at Stanford University for sponsoring the research reported in this paper.

## References

[1] Michael J. Caruso. Application of Magnetoresistive Sensors in Navigation Systems. In *Sensors and Actuators, 1997*, pages 15 – 21. SAE, 1997.

[2] Nathaniel Bowditch. *The American Practical Navigator*. Defense Mapping Agency, Hydrographic/Topographic Center, Bethesda, Maryland, USA, 1995.

[3] C.E. Barton. Revision of International Geomagnetic Reference Field Release. *EOS Transactions*, 77(16), April 1996.

[4] Arthur Gelb. *Applied Optimal Estimation*. M.I.T. Press, Cambridge, Massachusetts, 1974.

[5] Robert F. Stengel. *Optimal Control and Estimation*, pages 392 – 407. Dover, New York, New York, 1994.

[6] G. T. Haupt, N. J. Kasdin, G. M. Keiser, and B. W. Parkinson. Optimal Recursive Iterative Algorithm for Discrete Nonlinear Least-Squares Problem. *AIAA Journal of Guidance Control and Navigation*, 19(3):643 – 649, May - June 1996.

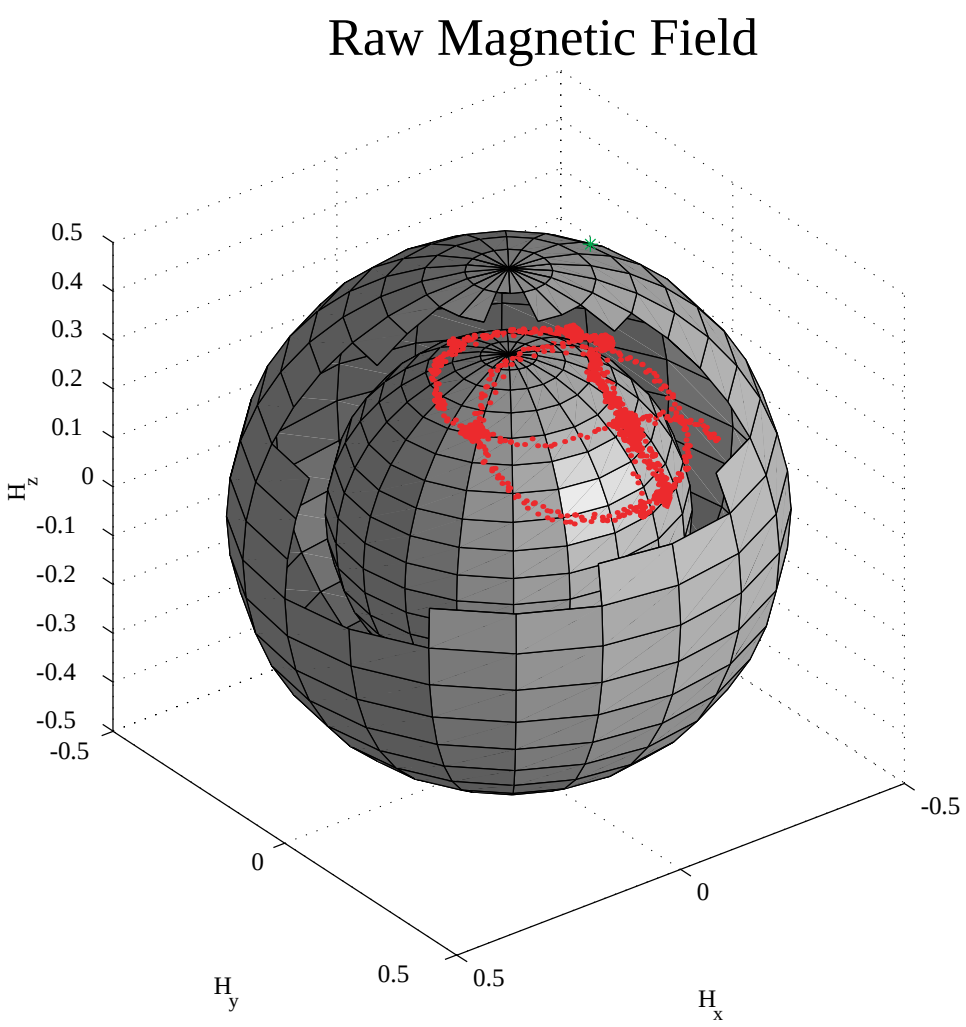


Figure 5: Locus of Measured Magnetic Field Before Calibration.

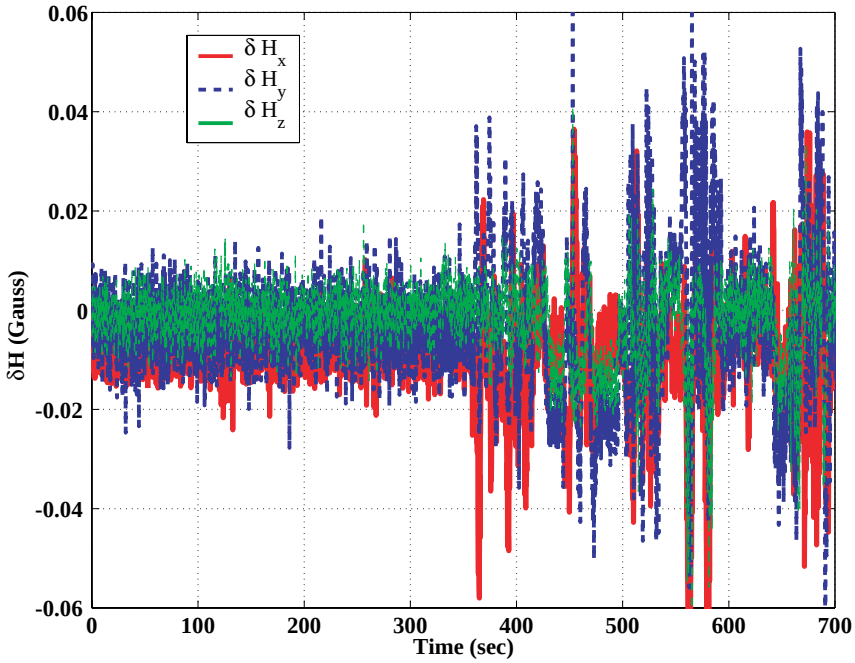


Figure 6: Magnetometer Calibration Residuals (for the first 700 seconds).

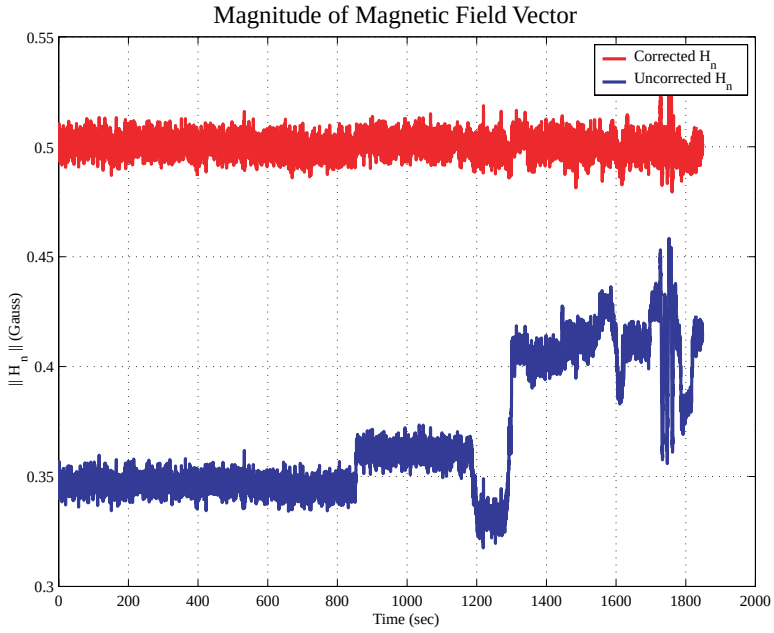


Figure 7: Pre- and Post Calibration Magnitude of Magnetic Field Measurements.